Green Synthesis of Piper nigrum Copper-based Nanoparticles: In-Silico Study and ADMET Analysis to Assess Their Antioxidant, Antibacterial, and Cytotoxic Effects

Y. Anusha
Yogi Vemana University Kadapa
Nambi Rajesh
Yogi Vemana University Kadapa
M. Vidya Vani
Yogi Vemana University Kadapa
Habeeb Khadri
Qassim University
Arifullah Mohammed
Universiti Malaysia
Khateef Riazunnisa
Yogi Vemana University Kadapa
Ashaimaa Y. Moussa (Ashaimaa_yehia@pharma.asu.edu.eg)
Ain shams University

Research Article

Keywords: Piper nigrum, PN-CuNPs, cytotoxicity, Molecular docking, Alkamides, ADMET/ TOPKAT, Antibacterial activity, Antioxidant activity

Posted Date: December 19th, 2022

DOI: https://doi.org/10.21203/rs.3.rs-1912885/v2

Abstract

Nano-biotechnology gained popularity and interest among scientists since it allowed for the green manufacturing of nanoparticles by employing plants as reducing agents. This method was safe, cheap, reproducible, and eco-friendly. In this study, the therapeutic potential of *Piper nigrum* fruit was mixed with the antibacterial activity of metallic copper to produce copper nanoparticles. The synthesis of copper nanoparticles was indicated by a colour change from brown to blue. Physical characterisation of PN-CuNPs was done by using UV-vis spectroscopy, FTIR, SEM, EDX, XRD and Zeta analyser. PN-CuNPs exhibited potential antioxidant, antibacterial and cytotoxic activities. PN-CuNPs showed improved free radical scavenging activity in a concentration dependant manner, reaching a maximum of 92%, 90% and 86% with DPPH, H_2O_2 and PMA tests. The antibacterial zone of inhibition of PN-CuNPs was the highest against *S. aureus* (23 mm) and the lowest against *E. coli* (10 mm), respectively. *In vitro* cytotoxicity of PN-CuNPs was demonstrated against MCF-7 breast cancer cell lines. The green synthesis of *P. nigrum* fruit was an excellent approach to produce PN-CuNPs with significant biological properties. Furthermore, more than 50 components of *Piper nigrum* extract were selected and subjected to *in-silico* molecular docking using the C-Docker protocol in the binding pockets of glutathione reductase, *E. coli* DNA gyrase topoisomerase II and EGFR tyrosine to discover their druggability. Pipercyclobutanamide A (26), pipernigramide F (32) and pipernigramide G (33) scored the best Gibbs free energy 50.489, 51.9306, 58.615 Kcal/mol, respectively. The ADMET/TOPKAT analysis confirmed the favourable pharmacokinetics, pharmacodynamics and toxicity profiles of the three promising compounds.

Introduction

Nanotechnology emerged as an interdisciplinary approach with various applications. Nanoparticles (NPs) emergence created scientific revolution for providing sustainable environment to humans [1]. NPs are auspicious due to their optical, catalytic, and surface to volume ratio [2, 3], and are currently being employed to treat a variety of ailments, as well as for energy storage and drug/gene delivery systems [4, 5].

Physical and chemical methods employed for the synthesis of NPs included lithography, ultrasonic fields, UV irradiation and photochemical reduction [6, 7], but these methods used hazardous chemicals as reducing agents. Hence, green synthesis of nanoparticles was introduced as an alternative method, which used either microbes or plant extract of medicinal plants as reducing agents. Green synthesis of nanoparticles by microbes is a time consuming process [8] for maintenance, but plant extract mediated process requires less time. Green synthesis of CuNPs by using plants was reported recently in *C. hirsutus* [9]; *Kigelia africana* fruit [10]; *Sesbania aculeta* [11]. Natural compounds act as an alternative for novel drug synthesis, and those that were plant-derived compounds showed high efficiency and easy availability [12]. Medicinal herbs had various bioactive molecules exhibiting various biological properties like antioxidant [13] antimicrobial [13], antibiofilm [14], antiquorum sensing [15] and antidiabetic [16–17]

Gold, silver, platinum, ruthenium, zinc and copper were various metals used for the synthesis of metal NPs [18–24]. Among these metal NPs, copper nanoparticles (CuNPs) were gaining popularity due to its distinctive properties like high surface area, low cost, and eco-friendliness nature. Physical characteristics of CuNPs included morphology, crystallinity, composition [25], simple methodology for synthesis, easy modification of CuNPs into required shape and size of CuNPs made the exceptional quality of CuNPs [26]. Biological activities of CuNPs prepared it as a source for antibiotic production as these are urgently needed [27, 28]. According to WHO, 177 ± 16 ppb is the permissible limit of copper [29], so folks used it to store food and drinking water. Copper vessels purify drinking water by killing *E. coli*, rapidly and efficiently destroy bacteria through a contact-killing mode [30].

Applying *In-silico* molecular docking to augment drug discovery research has gained much scientific interest during the previous years. Not only did it save time and effort spent on inactive molecules, but also resources are spared to proceed with promising drug entities further up to clinical stages. Virtual screening permitted the use of chemical structures of literature compounds compiled from eminent databases, filtered, and prepared to adopt a proper experimental design to predict the activity inside the binding pockets of certain enzymes.[31]. *Piper nigrum*, also known as pepper, is a member of the Piperaceae family. It is considered as “king of spices” [32]. *P. nigrum* seed is used as an acceptable food additive [33]. Piperine, is an alkaloid responsible for pungent odour used in traditional medicine and as an insecticide and with anticonvulsant properties. Phytochemicals present in black pepper includes phenols, flavonoids, alkaloids, amides, essential oils, lignans, neolignans, terpenes, chalcones etc [34] [35]

The water extract obtained from *Piper nigrum* fruits was shown to be rich in pungent principles as alkamides and piperine alkaloids; thus, these compounds were assembled from literature to perform the virtual screening. The same crude extract was utilized in all the bioassays described herein. Literature search manifested more than 55 compounds isolated from *Piper nigrum* fruits together with volatile metabolites. Due to the presence of biologically active components, they are as used natural therapeutic agents against bacterial, cancer, and fungal cells [36–38]. Various bioactivities were correlated with the alkaloids/alkamide components [39]; particularly, piperine. While 1% of piper fruits comprised essential oils, dominated by α-pinene, gluulol, α-terpinene, and *β*-caryophyllene, 5–9% represented pungent principles alkamides. In this study, about 60 compounds of alkamides/alkaloids and their derivatives were selected to investigate their binding properties and potential as antioxidants, antibacterial and antitumor agents. Furthermore, ADME/ TOPKAT analysis was conducted to reveal their pharmacokinetic properties, pharmacodynamics and toxicity.

Selected molecules for the *in-silico* study were as follows: the active chemosensate components in black pepper, sharing piperidine, pyrrolidine and isobutyl amide group, and classified as two categories of amides: the piperonal moiety associated amides and the long chain fatty acid unsaturated amides. [40] The anti-inflammatory alkamides pipernonaline, guineensine, pellitorine, retrofracamide C, piperrolein B, (2E,4Z,8E)-N-[9-(3,4-methylenedi- oxyphenyl)-2,4,8-nonatrienoyl]piperidine, piperchabamide D, dehydropipernonaline, retrofracamides, and pipernigramides, were included as well. (Figs. 1, 2 & 3) [41] [42 [43, 44, 45].

Piperine, the well-known alkaloid isolated from Piper more than hundreds of years ago, showed the lowest threshold of pungency followed by piperyline and piperettine. Indeed, the isobutyl amine and pyrrolidine containing compounds revealed higher threshold than any of the piperidine analogues. [40] Some of these compounds, like piperonylamine, pipericide, sarmentosine, sarmentine, chavicine are bioactive compounds having pharmacological effect (Fig. 1) [46]. In particular, piperine is believed to be the main bioactive chemical component with antimicrobial activities purified from *P. nigrum* [47].

Phytochemicals present in the *P. nigrum* fruit extract might be involved in reduction and stabilization of CuNPs synthesis. Therefore, the current study focuses on green synthesis of *P. nigrum* fruit-based copper nanoparticles using aqueous *P. nigrum* fruit extract, as well as their physical and biological characterisation. Moreover, molecular docking study was performed on the key active compounds in black pepper to manifest their druggability in the active sites of Epidermal Growth Factor Receptor (EGFR), DNA gyrase topoisomerase II and glutathione reductase.

Materials And Methods

Piper nigrum **fruit collection and preparation of fruit extract**

Piper nigrum fruits were purchased from the local market at Anantapur, Andhra Pradesh, India. Fruits were washed, shade dried, and powdered before being used. 10 grams of powdered *P. nigrum* was mixed with 100 ml of double distilled water and boiled in water bath at 70–80 ^{o}C for 15–20 min. The solution was cooled and filtered using Whatman No: 1 filter paper. The filtrate solution was then stored at 4$^{\circ}C$for further analysis.[39]

India is the major producer of *Piper nigrum* fruit and it is not an endangered species, therefore no government permission was required. Fruit sample was collected from the local market, Kadapa, Andhra Pradesh. A voucher specimen of *Piper nigrum* fruit was deposited and authenticated by Dr. A. Madhusudhana Reddy, Head of Herbarium Division, Dept. of Botany, Yogi Vemana University, Kadapa, India (Voucher specimen number of Piper nigrum fruit is YVU/KR-5301-5302).

Synthesis of P. nigrum **fruit extract copper nanoparticles (PN-CuNPs)**

PN-CuNPs were synthesized by adding 10 ml of fruit extract drop wise to the 200 ml of copper acetate solution and stirring with magnetic stirrer. The colour change of the solution from brown to blue represents the formation of PN-CuNPs. The reduction of copper ions was monitored by employing UV-visible spectrometer (Thermo scientific Evolution 201) with a wavelength range 200–800 nm. The reaction mixture was centrifuged at 10,000 rpm for 10 min and the pellet was washed with distilled water and air dried. The synthesized PN-CuNPs were stored for further analysis.

Characterisation of PN-CuNPs

UV-vis spectrophotometer

The absorption maxima of 2 ml of freshly prepared reaction mixture of PN-CuNPs was obtained by using UV -Vis spectrophotometer (Thermo scientific Evolution 401). The spectra were recorded with a wavelength range of 200 to 800 nm at regular time intervals (10, 15, 30, 45, 30, 45, 60, 120, and 180 min) by using double distilled water as a blank.

X-ray Diffraction (XRD) analysis of PN-CuNPs

XRD analysis of PN-CuNPs was performed on a PANLytical 'X' Pert PRO diffractometer operated at 40 kV and 30 mA with cu kα radiation. The average size of PN-CuNPs can be calculated using the Debye-Scherer equation.

$D = k\lambda/\beta\cos\theta$

Where D mention the crystallite size of the copper nanoparticles, λ the wavelength, β denote full width at half maximum of the diffraction peak, k denote as Scherer constant with a valve from 0.9-1 and θ denote as Bragg angle.

FTIR analysis of PN-CuNPs

Dehydrated PN-CuNPs and *P. nigrum* fruit extract were used to analyze functional groups.

10 mg of PN-CuNPs and *P. nigrum* fruit extract were mixed with 100 mg of KBr and vigorously ground into a fine powder and compressed into diaphanous pellet discs followed by FTIR [Perklin-Elmer (Spectrum Two model), UK Vertex 70 model, Bruker, German]. Chemical and functional groups of the samples were obtained in the range of 400 to 4000

cm^{-1} at room temperature. The probable biomolecules responsible for reduction, capping, and effective stabilization of the PN-CuNPs were recorded using FTIR spectrophotometer [48].

SEM and EDAX analysis of PN-CuNPs

Morphology and chemical composition of PN-CuNPs were examined by scanning electron microscopy (Model: EVO 18; Carl Zeiss, Germany) equipped with energy dispersive X-ray spectrometer (EDX). EDX was carried out at an acceleration voltage 20–40 keV. Thin films of PN-CuNPs were placed on a gold coated grid by just dropping a very small amount of PN-CuNPs on the grid. Thin films on SEM grid were dried for 5 min and examined at different angles.

Particle size and zeta potential determination

PN-CuNPs zeta potential and size was measured by zeta sizer nanoseries between 0.1 to 10,000 nm (Malvern Nano-ZS90). Stability of the nanoparticle sample was measured by maintaining the temperature of 25°C dispersion, 0.894 mPa of dispersion medium viscosity, 0.073 mS/cm conductivity with 3.8 V electrode voltages.

In-vitro antioxidant assays

DPPH free radical scavenging assay of P. nigrum fruit extract and PN-CuNPs

The biosynthesized PN-CuNPs and *P. nigrum* fruit extract were subjected to DPPH method. Different concentrations of PN-CuNPs and fruit extract (25–150 µg/ml) were mixed with 3 ml of methanolic solution containing DPPH radicals (0.1 mM). Ascorbic acid was taken as positive control. After 30 min, absorbance was determined at 517 nm and converted into % by the given formula. (Fig. S1).

% of inhibition = $[A_0\text{-}A_1/A_0] \times 100$

Where A_0 = Absorbance of control, A_1 = Absorbance of test

Hydrogen peroxide scavenging assay of P. nigrum fruit extract and PN-CuNPs

A modified protocol of Pavithra et al [49] was used for H_2O_2 scavenging assay. Different concentrations of (25–150 µg/ml) PN-CuNPs and *P. nigrum* fruit extract were mixed with 40 mM H_2O_2 solution, allowed to incubate for 10 min and the absorbance was measured at 230 nm. A positive control of ascorbic acid was used.

% of scavenging (H_2O_2) = $[A_0\text{-}A_1/A_0] \times 100$

Where A_0 = Absorbance of control A_1 = Absorbance of test

Phosphomolybdenum assay of P. nigrum fruit extract and PN-CuNPs

A modified protocol of Pavithra et al., [49] was used to estimate the total antioxidant activity. Molybdate reagent solution was prepared by 0.6 M sulphuric acid, 28 mM sodium phosphate and 4 mM ammonium molybdate. Different concentrations of PN-CuNPs (25–150 µg/ml) and *P. nigrum* fruit extract were added to each test tube individually containing 3 ml of distilled water and 1 ml of molybdate reagent solution followed by incubation in water bath at 95 ^{o}C for 90 min. After incubation, these test tubes were cool down to room temperature for 20–30 min and the absorbance was measured at 695 nm with ascorbic acid as positive control.

Antibacterial activity of P. nigrum fruit extract and PN-CuNPs

The antibacterial activity of PN-CuNPs and *P. nigrum* fruit extract was examined using the agar well method. *Staphylococcus aureus, Bacillus subtilis*, *Escherichia coli, Proteus vulgaris* were chosen to investigate the antibacterial efficacy of PN-CuNPs and *P. nigrum* fruit extract. Different concentrations (25, 50, 75 and 100 µl) of PN-CuNPs and *P. nigrum* fruit extract were used along with positive control

Ampicillin. Plates were incubated at 37 ^{o}C for 24 h and diameter of antibacterial zone of inhibition was measured.

Cytotoxicity of P. nigrum fruit extract and PN-CuNPs

The cytotoxicity of synthesized PN-CuNPs and *P. nigrum* fruit extract against MCF-7 cells was measured by MTT assay (Cell lines were purchased from the National Centre for Cell Science (NCCS), Pune, India). MCF-7 cells were seeded at a density of 5×10^4 cells/well in 96-well plates, then treated with various concentrations of PN-CuNPs and *P. nigrum* fruit extract (25–300 µg/ml) and incubated at 37°C for 24 hours at 5% CO_2 and 95% humidity. The cells were treated with MTT (5 mg/ml) and the absorbance was recorded at 570 nm.

In-silico molecular docking studies of piper bioactive compounds in EGFR, DNA gyrase and glutathione reductase

Fifty-eight compounds were selected from literature as the most bioactive components of *Piper nigrum* fruits, to be exact alkamide/alkaloids. The molecular docking was designed to be in the binding sites of three proteins: the glutathione reductase (Pdb ID:1Xan), DNA gyrase (Pdb ID:1kzn) and Epithelial Growth Factor Receptor EGFR (Pdb ID:1m17). The X-ray crystal structures were downloaded from the Protein Data Bank (PDB) website (https://www.rcsb.org/), with their binding native ligands, HXP xanthene, clorobiocin and erliotinib, respectively. The 3D chemical structures of the tested molecules and native ligands were prepared, and energy minimized by MMFF94x force field using our previous protocol (Ashaimaa Y. Moussa, Sobhy, Eldahshan, & Singab, 2020). The computational study was performed using the Discovery studio 4.5 software in Ain Shams University, Faculty of Pharmacy where ligands and enzymes were prepared using the molecular docking C-Docker protocols [50–52]

By employing the pH ionization mode to 7.5, the physiological state is best matched and simulated with respect to the types of conformers, isomers or tautomer produced; accordingly, the ligands Lipinski filter is adjusted. Root Mean Square Deviation (RMSD) value was calculated for the docking poses and found to be 1.0, which proved the accuracy of the reproduced poses and validated the docking process. This was accomplished by removing the co-crystallized ligand from the active site and superimposing the (experimental) with the docked native ligand (calculated).

The *in-vitro* standards ampicillin, ascorbic acid and doxorubicin were docked in their respective binding pockets to better assess and compare the significance of the ligands binding interactions and free energy. To simulate the biological After docking visualization was conducted using the Discovery Studio Visualizer 2022 where the top 10 poses were selected for each tested molecule according to the Gibbs free energy. Preferences were given between molecules according to their interaction similarity, covalent and noncovalent, with the binding ligands and standards. The binding Gibbs free energy was obtained from the following formula and per an implicit solvation model to present the best poses

$$\Delta G_{binding} = E_{complex} - (E_{protein} + E_{ligand})$$

$\Delta G_{binding}$ denoted: the binding energy of ligand–protein interaction.

$E_{complex}$: denoted: the potential energy for the complex of ligand bound with the protein.

$E_{protein}$ denoted: the protein potential energy only.

E_{ligand} denoted: the ligand potential energy only.

Results And Discussion

Synthesis of PN-CuNPs

The colour change from brown to blue validated the synthesis of PN-CuNPs. This was mediated by *P. nigrum* fruit extract, which is involved in the reduction of Cu^{+} to Cu°. UV-visible spectral analysis revealed a strong peak at 500 nm due to surface plasmon resonance (Fig. S2) [53–55]. Secondary metabolites like alkaloids, essential oils, polyphenolic compounds, terpenoids etc acted as stabilizing and capping agent and may be responsible for the reduction of Cu^{+} to Cu^{0} [53].

Characterization of PN-CuNPs

UV-vis spectrophotometer analysis of PN-CuNPs

Cooper solution was turned from brown to blue color after the addition of *P. nigrum* fruit extract powder, which indicated the synthesis of PN-CuNPs (Fig. S4). Due to surface plasmon resonance of CuNPs, colour change has occurred [54, 55].

X-ray Diffraction (XRD) analysis of PN-CuNPs

The crystalline nature of the PN-CuNPs was characterized by XRD analysis. The crystalline nature of synthesized PN-CuNPs was presented in Fig. S5. PN-CuNPs showed clearly face centered cubic (FCC) structure. The diffraction intensities were recorded from 20–80 values at 2θ range. Five characteristic peaks were observed at 2θ range of 38.32º, 44.47º, 64.66º and 77.55º were well matched with their corresponding Miller indices (111), (200), (220) and (311) corroborating with the values of the JCPDS card (card no. 89- 5899)13 (Fig. S5). The average crystalline size of CuNPs at all diffraction peaks were calculated by using Debye-Scherrer formula as $D=\frac{0.9\lambda}{\beta\cos\theta}$ nm. Here, crystalline size of PN-CuNPs is D, X-rays source wavelength λ (0.154 nm), full width of half maximum of diffraction peak is β and bragg angle θ. The average size of PN-CuNPs crystal is about 14 nm through green synthesis. The above results are consistent with [53, 56].

FTIR analysis of PN-CuNPs

FT-IR data of PN-CuNPs represents probable functional groups of phytochemicals involved in bio-reduction as well as stabilisation of PN-CuNPs (Fig. S6 and Table S1). $3801cm^{-1}$ absorption band of PN-

CuNPs corresponds to O-H stretch of alcohol. 3377 cm^{-1} absorption band of PN-CuNPs corresponds to N-H stretching which represents to aliphatic primary amine functional groups. 2366 and 2307 cm^{-1} band corresponds to C–H of alkyne. 1522 cm^{-1} band corresponds to aromatic C–H, C = C functional groups. 1408 cm^{-1} absorption band of PN-CuNPs corresponds to asymmetric stretching. The alkaloids, essential oils, polyphenolic compounds, terpenoids etc and other phytochemicals present in the *P. nigrum* were involved in the bio-reduction of Cu^{+} to PN-CuNPs [48, 57].

SEM and EDX spectral analysis of PN-CuNPs

External morphology of PN-CuNPs was observed through SEM (Fig. S7A). It forms a spindle shaped structure. Elemental analysis of PN-CuNPs was investigated by Energy Dispersive X-ray Analysis (EDX) (Fig. S7B) at 1 and 8 keV. It displays the percent and composition of Cu metal as significant peak and other small peaks corresponds to biomolecules capping the PN-CuNPs. Fig. S7B illustrates the percentages of Cu and other elements.

Particle size and zeta potential determination of PN-CuNPs

PN-CuNPs hydrodynamic size and surface charge were revealed by particle size analyzer and zeta potential analyser. PN-CuNPs average diameter was 30–32 nm with negative surface zeta potential (– 50 mV) and remained constant over a period confirming the stability and the strong repulsion among the particles (Fig. S8A & S8B). This observation can be attributed to the presence of biomolecules as stabilizing agents in the leaf extract. The zeta potential measures the surface charge of particles. As the zeta potential increases, the surface charge of the particles increased. The zeta potential greatly influences particle stability in suspension through the electrostatic repulsion between particles. Our results are consistent with [46, 47].

In-vitro antioxidant assays

Free radical scavenging assay of P. nigrum fruit extract and PN-CuNPs

PN-CuNPs and *P. nigrum* fruit extracts were subjected to DPPH assay. PN-CuNPs showed the elevated % of DPPH free radical scavenging activity compared to *P. nigrum* fruit extracts. Elevated concentration of PN-CuNPs resulted elevated % of free radical scavenging activity. PN-CuNPs showed highest % of inhibition of about 92% at 250 µg/ml concentration (Fig. S1& S9A, Fig. S9) [58, 59].

Hydrogen peroxide scavenging assay of P. nigrum fruit extract and PN-CuNPs

PN-CuNPs and *P. nigrum* fruit extract were examined for their H_2O_2 free radical scavenging activity. PN-CuNPs showed the elevated percent of H_2O_2 free radical scavenging activity compared to *P. nigrum* fruit extracts. Increasing concentration of PN-CuNPs yielded elevated % of free radical scavenging activity. PN-CuNPs showed highest percentage of inhibition of about 90% at 250 µg/ml concentration (Fig. S9B).

Total antioxidant activity (TAA) of P. nigrum fruit extract and PN-CuNPs

PN-CuNPs and *P. nigrum* fruit extracts were subjected to determine the TAA by phosphomolybdenum method. PN-CuNPs exhibited the increased percent of free radical scavenging activity compared to *P. nigrum* fruit extracts. Increasing concentration of PN-CuNPs resulted higher percentage of TAA. TAA of PN-CuNPs ranged from 68 to 86%. PN-CuNPs showed highest 86% of TAA at 250 µg/ml concentration (Fig. S1 & S9C).

Antibacterial activity of P. nigrum fruit extract and PN-CuNPs

PN-CuNPs and *P. nigrum* fruit extracts were scrutinized to antibacterial activity by agar well diffusion method against human pathogenic microbes such as *S. aureus, B. subtilis, E. coli* and *P. vulgaris*. PN-CuNPs showed highest antibacterial zone of inhibition with increasing concentration. Antibacterial zone of inhibition was in the range of 10 ± 0.17 to 23 ± 0.52 mm (Fig. S10A-D, Fig. S2& S11). *S. aureus* exhibited maximum antibacterial zone of inhibition of about 23 ± 0.52 mm (Fig. S10A) at 100 µg/ml concentration and minimum zone of inhibition was found with *E. coli* (10 ± 0.17 mm) at 25 µg/ml as depicted in Fig. S10C respectively. Hence *S. aureus* was more susceptible bacterial for PN-CuNPs [59, 60].

Proposed mechanism of antibacterial activity of PN-CuNPs

PN-CuNPs exhibited highest antibacterial zone of inhibition against Gram + ve bacteria like *S. aureus* compared to Gram-ve bacteria. Copper is an essential metal for growth of microbes at lowers concentration but at higher concentration it will inhibit growth of bacteria by penetrating the bacterial cell wall. The Cu^{+} ions of PN-CuNPs penetrate into bacterial cell wall and ceases growth of bacteria. Size and shape of CuNPs influences the antibacterial activity. Free surface energy of the particles changes with size and morphology, finally pH inside the cells [61]. The proposed mechanism of action of antibacterial activity of PN-CuNPs was depicted in Fig. S11 Mechanism of action of PN-CuNPs occurs by enzyme interaction with –SH groups leading to DNA damage and finally generation of oxidative stress leading to ROS production [62, 63]. ROS species changes redox properties of copper which causes toxicity for bacterium, which is induced by Cu^{+1} and Cu^{+2} ions [64, 65], finally leading to antibacterial effect.(Fig S11)

Cytotoxicity assay of P. nigrum fruit extract and PN-CuNPs

CuNPs has wide range of biomedical applications in medicine, drug delivery and anti-angiogenic property of cancer. PN-CuNPs and *P. nigrum* fruit extracts were subjected to cytotoxic effect against breast cancer cell line MCF-7 by MTT assay. PN-CuNPs exhibited cytotoxicity against cancer cells. At 200 µg/ml, PN-CuNPs showed cytotoxic activity of about 80% against MCF-7 cell line (Fig. S12). The results shown in Fig S12 indicated that PN-CuNPs caused a significant decrease in cell viability of the MCF-7 cells when compared to the *P. nigrum* fruit extract [27, 66].

Anticancer activity of green synthesized CuNPs by medicinal plants was confirmed by previous studies [67–69]. In the study of Suman et al. [68] clarified HeLa cell line was suppressed at the high doses of *Morinda citrifolia* metallic NPs. *Piper longum* leaf extract NPs inhibited Hep-2 cell lines [70]. *Annona squamosa* leaf extract NPs suppressed MCF-7 cell line [71]. CuNPs anticancer property was influenced by size, form, and surface coating of NPs. Size of CuNPs influences most among all parameters [72].

Proposed mechanism of cytotoxicity activity of PN-CuNPs

Significant anticancer potentials of PN-CuNPs synthesized by *P. nigrum* fruit extracts against common MCF-7 breast cancer cell lines are linked to their antioxidant activities. Previous similar studies, revealed that CuNPs and medicinal plants reduced tumours by supressing free radicals [71]. Free radicals induced mutations in DNA and RNA, resulting in altered gene expression finally leading to cancerous cells proliferation [72]. The free radicals at elevated levels in the various organs led to angiogenesis and tumorigenesis [73]. The proposed mechanism of action of cytotoxic activity of PN-CuNPs was depicted in Fig. S13. Medicinal plant based PN-CuNPs removed free radicals as well as inhibited cancer cells growth [74]. In the current study, cell viability of MCF-7 cells was reduced, suggesting anticancer activity of PN-CuNPs. To understand the in-detailed mechanism further studies are required. Fig S13.

Docking Interactions

To virtually investigate the potential of the selected compounds as antioxidants, glutathione reductase was utilized as a binding enzyme. It is responsible for providing the reduced glutathione to most of the cells and controlled reactive oxygen species.

Four compounds pipernigramide F 32, pipercyclobutanamide A 26, guineensine 10, and brachyamide A 40 reported the best binding free energy in the glutathione reductase enzyme as non-competitive inhibitors by fitting allosterically to the NADPH/FAD binding pocket. The scored ΔG values were 40.18, 41.83, 38.58, 42.03 Kcal/mol, respectively, while the control ascorbic acid scored 25.31 Kcal/mol. The key amino acid residues involved in the non-covalent interactions were Asn71, His75 and His82 with both the native ligand HXP xanthene and ascorbic acid. Pipernigramide F 32 manifested seven firm interactions with the vital amino acid residues in the active site through its cyclobutane, and aromatic rings together with the proton acceptors as the dioxole and carbonyl moieties detailed as: π - π -stacked bond with His75, C-H bond with His82, π -alkyl bonds with His 82, Trp70 and Phe82, conventional H bond with Asn71 and π - π T shaped bond with Tyr407 (Fig. 4). Pipercyclobutanamide A 26 revealed eight non-covalent binding modes, which were π-sigma bonds with Phe78, three π-alkyl bonds with Phe78, Leu 438, Val 74, and Tyr407, C-H bonds with His75, π-donor H-bonds with His82 and conventional H bonds with His 75. Guineensine 10 showed several desirable interactions as five π -alkyl bonds with Tyr407, His82, Leu438, Val74, Trp70, one pi- pi stacked bond with Phe78, two conventional H-bonds with Asn71 and His75 and one Pi-sigma bond with Phe78.

Brachyamide A 40 demonstrated π - π stacked bonds with Phe78, C-H bonds with Glu77, His75, Tyr407 and His82 as well as alkyl bonds between the hydrophobic residues Leu438, Val74, Phe78 and the respective nonpolar portions of the ligand. Additionally, Van der Waals forces were revealed with Tyr407.

Regarding the *E. coli* DNA gyrase topoisomerase II (1Ksn), its importance was clear as it was involved in maintaining the chromosomal superhelicity in the microbial transcription and replication processes. While the B subunit of 1Ksn molecule encompassed the ATPase active site in the N-terminal domain, the C-domain interacted with the DNA to alter the superhelical form of the DNA substrate. Due to the rise in the number of resistant microbial strains encountered, new inhibitors of the gyrase enzyme were desperately needed. Herein, the docking of the selected *Piper nigrum* fruit components was performed in the ATP hydrolysis binding site, and the amino acid residues with the most influence, as detailed and described by [75] were D73, and N46 reported to synchronize with Mg^{+2} in the ATP binding site. The best binding bioactive compounds in the DNA gyrase active site were pipernigramide G 33, pipnoohine 25 and pipercyclobutanamide A 26, and Pipernigramide G 33. The amide group in compound 33 interacted through nine non-covalent bonds; conventional H bond with Lys99, the aromatic and saturated rings exhibited four alkyl interactions with Ala86, Pro79, Val167, and Ala47, Van der Waals (VDV) forces between Arg136 and the dioxole ring. C-H bond with Arg76 and between proton donors and Asp101 was recorded in the DNA gyrase pocket as well as π-anion interaction with Asp 49. The ΔG binding energy was − 58.615 Kcal/mol, which was of superior activity than the positive control ampicillin (-49.407 Kcal/mol). (table 1)

Pipnoohine 25 revealed conventional H-bond between Arg136 and the amide group. Alkyl interactions between the hydrophobic side chain, Ala86 and Pro79 were detected.

Pipercyclobutanamide A 26 showed conventional H bond with Gly77, π-anion interaction between Glu50, Arg76 and the aromatic ring. Pro79, Ile78, Ile90, Ala86 and Arg76 were involved in alkyl type interactions with unsaturated and saturated rings. π - π T shaped between Phe50 and the benzo dioxole ring. C-H bond between Asp73, Asn46 and Asp49 and proton donors.

The core interacting residues in the standard ampicillin within 3°A were conventional H-bond between the amine group and residue Asn46, attractive charges between Lys99 and the acidic anions, VDV forces and alkyl interactions with Ile78 and Asp49. The afore-mentioned amino acids comparably interacted with the selected compounds; especially, pipernigramide G 33, pipnoohine 25 and pipercyclobutanamide A 26 confirming their potential potency as antimicrobial agents.

As far as EGFR tyrosine kinase (1m17) was concerned,[76] the docking study was carried out in the same active site, the ATP binding site, as the native co-crystallised ligand erlotinib, a major tyrosine kinase inhibitor approved by the FDA. After careful analysis, the binding modes of the two compounds pipernigramide G 33 and pipernigramide F 32 (Fig. 4) proved to be promiscuous and scored the lowest Gibbs free energy, 54.1347 and 62.1958 Kcal/mol respectively, with a minus sign indicating the quick auspicious fitting in the EGFR binding pocket, which is even better than erlotinib whose free energy was 47.3483 Kcal/mol. (table 1) Within a measured distance of 2°A, compound 33 showed conventional H bond formation between the residues Lys 721, Asp831, Thr830, and Thr766 and its amide carbonyl group. This was evident also between Met769 and the oxygen atom of the dioxole rings.

Four alkyl interactions between the aromatic moiety and four amino acid residues Val702, Leu820, Ala719, and Leu694 stabilised the binding of the molecule over the hydrophobic bed. VDV forces between the piperdine protons and Pro770 added more to the nonpolar favourable interactions; additionally, π-donor hydrogen bond between Cys773 and the hydrophobic aromaticity, and the C-H bond detected between Glu738 and proton donors of the piperdine ring were identified.

The lowest scored ΔG value was reserved to pipernigramide F 32 (Fig. 4) with interaction forces as follows: π-sulphur bond between Cys773 and the aromatic rings. Conventional H bonds between the benzo dioxole ring and Lys721, Met769, Thr830, and Thr766. Three C-H bonds with Pro770 and Glu738. Alkyl interactions between the piperidine ring and Val702, Ala719 and Gly772. C-H bond was noticed between the Gly695 and the dioxole ring. Moreover, Asp831 interacted through a C-H bond with protons of piperdine ring.

The main vital forces responsible for bioactivity were the number of different interactions, their types, bond distance measured, and strength as compared to the ligand erlotinib. Erlotinib good binding affinity comprised of its unique interactions, namely, salt bridge formation with Asp831, alkyl interactions with Lys721 and Met742, Leu 820 and Val720 as well as H bond with Cys773. VDV forces contributed to a firmer binding through Gly695, Glu738 and Leu694, all within a distance less than 2°A. comparable interactions were identified in the bioactive compounds; particularly, pipernigramide F 32 and pipernigramide G 33 suggesting their promising potential as antitumor agents with tyrosine kinase inhibition activity.

The vital factors that contributed to better binding forces and whose significance was most noted were the length of the molecule in terms of the number of carbons in the side chain; for instance, 26 was of firmer binding energy than pipernigramide F 32 owing to the only difference between them, which was the side chain length. Secondly, the presence of the piperidine ring improved fitting into the enzyme pocket as it is shown by comparing the ΔG value of brachyamide A 40 and guineensine 10 even the unsaturation in a single bond contributed to a noticeable decrease in binding strength as it was clear in the pairs of compounds, 4/5, 16/17 and 13/14. Moreover, the size of the molecule and its orientation in the active site proved to be of considerable importance as it is evident from the smallest three docked molecules piperonal 24, 1-nitrosoimino-2,4,5-trimethoxybenzene 42, 3',4'-methylenedioxycinnamaldehyde 45, and sarmentosine 49 whose binding forces were the least compared to their congeners. It appeared that appropriate contact with the hydrophobic bed was essential for achieving the best possible binding interactions, which required either long chain molecule or a multicyclic structure; additionally, pyrrolidine was favoured than the piperdine ring as observed from the two compounds 1-piperettylpyrrolidine 36 and piperoleine 37. The standard ascorbic acid proton acceptor groups showed conventional hydrogen bonds with His 75, Asn71, and His 82, which highlighted the core value of the number of proton acceptors in the binding ligand. It is worth mentioning that the best fitting compounds 32, 26, 10 and 40 manifested the same types of interactions with the amino n acid residues. Similarly, the native ligand HXP xanthene revealed analogous type of interactions to the control ascorbic acid.

ADMET and TOPKAT analysis

ADMET prediction of the selected alkamides indicated their pharmacodynamic, pharmacokinetic, and toxicity properties (Table 3). The cytochrome inhibition was reported for only few compounds as well as the hepatoxicity profile. Penetration levels in blood brain barrier (BBB) were ranked from 0 to 4, from the very high penetration to the least levels, respectively. In the same way, absorption was expressed on the scale 0, 1, 2, and 3 indicating good, moderate, low and very low absorption levels. The most potent compounds revealed a BBB penetration level of 4 with true or more than 90% binding to plasma proteins, indicating its promising drug likelihood. (Table 3)

Moderate absorption for pipernigramide E 31, F 32, and G 33, yet pipercyclobutanamide A 26 manifested very low absorption score. The solubility score of 2 indicated low solubility for the compounds pipernigramide E 31, F 32, and G 33, and pipercyclobutanamide A 26, which possibly require suitable formulation to assist delivering to the active site. Most of the alkamides tested revealed moderate intestinal absorption characteristics as evidenced by the ADMET plot in Fig. 5 where they were in the 99% absorption ellipse with only compounds 52–54 located outside the 99% absorption range. The BBB penetration with values 0 and 1 was either very high or high penetration except for compounds 35–39 lying outside the 99% confidence ellipse of BBB absorption (Table 3. and Fig. 5.). Regarding the plasma protein binding, most of the compounds showed binding more than 90% except for 1, 2, 7, 12, 15, 18, 29, 36, 37, 39, 42, 51 and 58.

The solubility levels of the chosen compounds were of values 2 or 3 indicating low to moderate solubility except for compounds 48 and 49 identified as being insoluble and of very low solubility levels. A few compounds manifested binding to CY2D6 such as 13, 14, 16, 17, 19, 55 and 21–24.

The TOPKAT analysis revealed that all the tested compounds were non-mutagenic and non-carcinogenic against male and female rats FDA except for 18, 20–22 and 54 (Table 2.). The LD50 measured orally in rats ranged between 0.11 and 4.81 g/kg body wt. whereas the lowest observed adverse effect level (LOAEL) values ranged between 0.296 and 0.0002 g/kg body wt. Ocular and skin irritancy were mild for most of the compounds.

Conclusion

The green synthesis of CuNPs using an aqueous extract of *P. nigrum* fruit extract was confirmed by UV-vis absorption, EDX analysis, FTIR spectrometry, and diffraction pattern XRD. The particle size of the synthesized PN-CuNPs was 30-32nm with zeta potential of about − 50 mV. This study demonstrated that both *P. nigrum* fruit extract and their synthesized PN-CuNPs displayed considerable antioxidant, antibacterial and antitumor activities. Virtual screening technique employed herein on more than 55 alkamide/alkaloid compounds using Discovery studio 4.5 software and the validated C-Docker protocol unveiled the promising free binding energies of most of the compounds, which was even superior compared to their native ligands and positive controls. Careful analysis of docking results manifested key amino acid interactions and binding forces as well as vital factors involved in structure binding

relationships. ADMET/ TOPKAT study indicated that the most potent compounds were of low toxicity and favourable pharmacodynamic and pharmacokinetic profiles.

Declarations

Authors contribution:

YN, experimental **NR**, biological assays **VV,** experimental and draft writing **HR**, revise **AM,** manuscript draft writing, revise and editing **KR**, conceptualization, supervision and validation **AYM,** experimental design, methodology**,** molecular docking, validation, manuscript draft writing, revise and editing, and conceptualization.

Ethics approval and consent to participate

Our experiments were totally based on in vitro studies using bacterial isolates and cell lines to evaluate the antibacterial and anticancer activity of piper fruit copper nanoparticles, therefore ethical review is not required. We confirm that all experiments were performed in accordance with the relevant guidelines and regulations. The appropriate authorization has been obtained for the collection of the fruit and its use has been carried out in accordance with the relevant guidelines. Identification of the plant was carried out by Dr. A. Madhusudhana Reddy, Head of Herbarium Division, Dept. of Botany, Yogi Vemana University, Kadapa, India. Our experimental methods do not contain human, animal and clinical data.

Consent for publication

Not applicable

Availability of data and materials

All the data are already released and included in this manuscript and its supplementary files. The datasets used or analyzed during the present study are available with the corresponding author upon reasonable request.

Acknowledgements

This research article is from the collaboration between Ain Shams University, Yogi Vemana University Kadapa, Qassim University, and Universiti Malaysia Kelantan. Many thanks to the laboratory assistants involved in this project. AYM is deeply grateful for the department of Medicinal chemistry in faculty of Pharmacy, Ain Shams University for providing the software used in the virtual screening and molecular docking part.

Funding

No external funding is received for this work.

Declaration of Competing Interest

The authors declare no conflict of interest.

References

1. I. Khan, K. Saeed and I. Khan, Arab J Chem **12** (7), 908-931 (2019).

2. J. Singh, T. Dutta, K.-H. Kim, M. Rawat, P. Samddar and P. Kumar, J nanobiotechnology **16** (1), 1-24 (2018).

3. G. K. Sarma, S. Sen Gupta and K. G. Bhattacharyya, Environ Sci Pollut Res **26** (7), 6245-6278 (2019).

4. C. N. Fries, E. J. Curvino, J.-L. Chen, S. R. Permar, G. G. Fouda and J. H. Collier, N Nanotech **16** (4), 1-14 (2021).

5. E. Pomerantseva, F. Bonaccorso, X. Feng, Y. Cui and Y. Gogotsi, Science **366** (6468), eaan8285 (2019).

6. F. Mafuné, J.-y. Kohno, Y. Takeda and T. Kondow, J Phys Chem B **106** (31), 7575-7577 (2002).

7. R. R. Naik, S. J. Stringer, G. Agarwal, S. E. Jones and M. O. Stone, Nat mater **1** (3), 169-172 (2002).

8. K. N. Thakkar, S. S. Mhatre and R. Y. Parikh, Nanomed Nanotechnol Biol Med **6** (2), 257-262 (2010).

9. S. Ameena, N. Rajesh, S. M. Anjum, et al., Appl Biochem Biotechnol 1-15 (2022).

10. I. I. Alao, I. P. Oyekunle, K. O. Iwuozor and E. C. Emenike, j chem Sect B **4** (1), 39-52 (2022).

11. V. Tamil Elakkiya, R. Meenakshi, P. Senthil Kumar, et al., Int J Environ Sci Technol **19** (3), 1313-1322 (2022).

12. G. M. Cragg and D. J. Newman, Biochim Biophys Acta **1830** (6), 3670-3695 (2013).

13. K. Mseddi, F. Alimi, E. Noumi, et al., Arab j chem **13** (8), 6782-6801 (2020).

14. M. A. Gad-Elkareem, E. H. Abdelgadir, O. M. Badawy and A. Kadri, PeerJ **7**, e6441 (2019).

15. M. Snoussi, A. Dehmani, E. Noumi, G. Flamini and A. Papetti, Microb Pathog **90**, 13-21 (2016).

16. E. Noumi, A. Merghni, M. M Alreshidi, et al., Molecules **23** (10), 2672 (2018).

17. Moussa, A Y, Labib, R. M., & Ayoub, N. A. (2013). Isolation of chemical constituents and protective effect of Pistacia khinjuk Against CCl 4 – induced damage on HepG2 Cells. 4(4), 1–9.

18. A. Folorunso, S. Akintelu, A. K. Oyebamiji, et al., J Nanostructure Chem **9** (2), 111-117 (2019).

19. S. A. AKINTELU, A. S. FOLORUNSO and O. T. ADEMOSUN, in *J drug deliv ther* (2019), Vol. 9, pp. 58-64.

20. Anjum SM, Riazunnisa K, Fine ultra-small ruthenium oxide nanoparticle synthesis by using Catharanthus roseus and Moringa oleifera leaf extracts and their efficacy towards in vitro assays, antimicrobial activity and catalytic: adsorption kinetic studies using methylene blue dye. J Cluster Sci 2021; https://doi.org/10.1007/s10876-021-02037-0..

21. Akintelu S, Folorunso A: Characterization and antimicrobial investigation of synthesized silver nanoparticles from Annona muricata leaf extracts. J Nanotechnol 2019; 6:1-5.

22. Akintelu SA, Folorunso AS, Oyebamiji AK, Erazua EA: Antibacterial potency of silver nanoparticles synthesized using Boerhaavia diffusa leaf extract as reductive and stabilizing agent. Int J Pharma Sci Res 2019; 10(12):374-38023. M. Nasrollahzadeh, S. Mahmoudi-Gom Yek, N. Motahharifar and M. Ghafori Gorab, Chem Rec **19** (12), 2436-2479 (2019).

23. Nasrollahzadeh M, Mahmoudi-Gom Yek S, Motahharifar N, Ghafori Gorab M: Recent developments in the plant-mediated green synthesis of Ag-based nanoparticles for environmental and catalytic applications. Chem Rec 2019; 19(12):2436-2479.

24. Almatroudi A, Khadri H, Azam M, Rahmani AH, Khaleefah A, Khaleefah F, Khateef R, Ansari MA, Allemailem KS: Antibacterial, antibiofilm and anticancer activity of biologically synthesized silver nanoparticles using seed extract of Nigella sativa. Processes 2020; 8(4):388.

25. Cuevas R, Durán N, Diez M, Tortella G, Rubilar O: Extracellular biosynthesis of copper and copper oxide nanoparticles by Stereum hirsutum, a native white-rot fungus from chilean forests. J Nanomater 2015; 2015.26. E. R. Balasooriya, C. D. Jayasinghe, U. A. Jayawardena, R. W. D. Ruwanthika, R. Mendis de Silva and P. V. Udagama, J Nanomater **2017** (2017).

26. Balasooriya ER, Jayasinghe CD, Jayawardena UA, Ruwanthika RWD, Mendis de Silva R, Udagama PV: Honey mediated green synthesis of nanoparticles: new era of safe nanotechnology. J Nanomater 2017; 2017.

27. I. M. Chung, A. Abdul Rahuman, S. Marimuthu, et al., Exp Ther Med **14** (1), 18-24 (2017).

28. Moussa, Ashaimaa Y, Lambert, C., Stradal, T. E. B., Ashrafi, S., Maier, W., Stadler, M., & Helaly, S. E. (2020). New Peptaibiotics and a Cyclodepsipeptide from Ijuhya vitellina : Isolation , Identification , Cytotoxic and Nematicidal Activities. Antibiotics, 1–13. https://doi.org/doi:10.3390/antibiotics9030132

29. V. P. Sudha, S. Ganesan, G. Pazhani, T. Ramamurthy, G. Nair and P. Venkatasubramanian, J Health Popul Nutr **30** (1), 17 (2012).

30. C. E. Santo, E. W. Lam, C. G. Elowsky, et al., Appl Environ Microbiol **77** (3), 794-802 (2011).

31. Ahmed E. Altyar 1, Fadia S. Youssef 2, Maram M. Kurdi 3, Renad J. Bifari 3 and Mohamed L. Ashour," The Role of Cannabis sativa L. as a Source of Cannabinoids

against Coronavirus 2 (SARS-CoV-2): An In Silico Study toEvaluate Their Activities and ADMET Properties" Molecules, 2022

32. Takooree H, Aumeeruddy MZ, Rengasamy KR, Venugopala KN, Jeewon R, Zengin G, Mahomoodally MF: A systematic review on black pepper (Piper nigrum L.): From folk uses to pharmacological applications. Crit Rev Food Sci Nutr 2019; 59(sup1):S210-S243.

33. Meghwal M, Goswami T: Piper nigrum and piperine: an update. Phytother Res 2013; 27(8):1121-1130.

34. Shityakov, S., Bigdelian, E., Hussein, A. A., Hussain, M. B., Tripathi, Y. C., Khan, M. U., & Shariati, M. A. (2019). Phytochemical and pharmacological attributes of piperine: A bioactive ingredient of black pepper. European Journal of Medicinal Chemistry, 176, 149–161. https://doi.org/10.1016/j.ejmech.2019.04.002

35. Yunbao Liu1, Vivek R. Yadev2, B. B. A. and M. G. N. (2014). Inhibitory Effects of Black Pepper (Piper nigrum) Extracts and Compounds on Human Tumor Cell Proliferation, Cyclooxygenase Enzymes, Lipid Peroxidation and Nuclear Transcription Factor-kappa-B. Natural Product Communications, 9(8).

36. Zhang C, Zhao J, Famous E, Pan S, Peng X, Tian J: Antioxidant, hepatoprotective and antifungal activities of black pepper (Piper nigrum L.) essential oil. Food chem 2021; 346:128845.

37. Reshmi S, Sathya E, Devi PS: Isolation of piperdine from Piper nigrum and its antiproliferative activity. J Med Plant Res 2010; 4(15):1535-1546.

38. Aldaly ZT: Antimicrobial activity of piperine purified from Piper nigrum. J Basrah Res 2010; 36:54-61.

39. Tyagi PK, Tyagi S, Gola D, Arya A, Ayatollahi SA, Alshehri MM, Sharifi-Rad J: Ascorbic acid and polyphenols mediated green synthesis of silver nanoparticles from Tagetes erecta L. aqueous leaf extract and studied their antioxidant properties. J Nanomater 2021; 2021.

40. Dawid, C., Henze, A., Frank, O., Glabasnia, A., Rupp, M., Büning, K., … Hofmann, T. (2012). Structural and sensory characterization of key pungent and tingling compounds from black pepper (Piper nigrum L.). Journal of Agricultural and Food Chemistry, 60(11), 2884–2895. https://doi.org/10.1021/jf300036a

41. Barata, L. M., Andrade, E. H., Ramos, A. R., De Lemos, O. F., Setzer, W. N., Byler, K. G., … Da Silva, J. K. R. (2021). Secondary metabolic profile as a tool for distinction and characterization of cultivars of

black pepper (Piper nigrum L.) cultivated in Pará State, Brazil. International Journal of Molecular Sciences, 22(2), 1–18. https://doi.org/10.3390/ijms22020890

42. S. Shityakov, E. Bigdelian, A. A. Hussein, et al., Eur J Med Chem **176**, 149-161 (2019).

43. Sook, Y., Sachie, Y., Shigeru, N., & Yuji, T. (2017). Piperine - like alkamides from Piper nigrum induce BDNF promoter and promote neurite outgrowth in Neuro - 2a cells. Journal of Natural Medicines. https://doi.org/10.1007/s11418-017-1140-3

44. Rho, M. C., Lee, S. W., Park, H. R., Choi, J. H., Kang, J. Y., Kim, K., … Kim, Y. K. (2007). ACAT inhibition of alkamides identified in the fruits of Piper nigrum. Phytochemistry, 68(6), 899–903. https://doi.org/10.1016/j.phytochem.2006.11.025

45. Scott, I. M., Puniani, E., Jensen, H., Livesey, J. F., Poveda, L., Sánchez-Vindas, P., … Arnason, J. T. (2005). Analysis of piperaceae germplasrn by HPLC and LCMS: A method for isolating and identifying unsaturated amides from Piper spp extracts. Journal of Agricultural and Food Chemistry, 53(6), 1907–1913. https://doi.org/10.1021/jf048305a

46. Majdalawieh AF, Carr RI: In vitro investigation of the potential immunomodulatory and anti-cancer activities of black pepper (Piper nigrum) and cardamom (Elettaria cardamomum). J Med Food 2010; 13(2):371-381.

47. Mohammed GJ, Omran AM, Hussein HM: Antibacterial and phytochemical analysis of Piper nigrum using gas chromatography-mass Spectrum and Fourier-transform infrared spectroscopy. Int J Pharmaco Phytochem Res 2016; 8(6):977-996.

48. Kanniah P, Chelliah P, Thangapandi JR, Gnanadhas G, Mahendran V, Robert M: Green synthesis of antibacterial and cytotoxic silver nanoparticles by Piper nigrum seed extract and development of antibacterial silver based chitosan nanocomposite. Int J Biol Macromol 2021; 189:18-33..

49. Pavithra K, Vadivukkarasi S: Evaluation of free radical scavenging activity of various extracts of leaves from Kedrostis foetidissima (Jacq.) Cogn. Food Sci Hum Wellness 2015; 4(1):42-46.

50. Nehal Ibrahim and Ashaimaa Y. Moussa. (2021). A comparative volatilomic characterization of Florence fennel from different locations: antiviral prospects. https://doi.org/10.1039/d0fo02897e

51. Abdel Razek, M. M. M., Moussa, A. Y., El-Shanawany, M. A., & Singab, A. N. B. (2020). A New Phenolic Alkaloid from Halocnemum strobilaceum Endophytes: Antimicrobial, Antioxidant and Biofilm Inhibitory Activities. Chemistry and Biodiversity, 17(10). https://doi.org/10.1002/cbdv.202000496.

52. Moussa, Ashaimaa Y., Sobhy, H. A., Eldahshan, O. A., & Singab, A. N. B. (2020). Caspicaiene: a new kaurene diterpene with anti-tubercular activity from an *Aspergillus* endophytic isolate in *Gleditsia caspia* desf. Natural Product Research, 1–12. https://doi.org/10.1080/14786419.2020.1824222

53. Ghosh MK, Sahu S, Gupta I, Ghorai TK: Green synthesis of copper nanoparticles from an extract of Jatropha curcas leaves: characterization, optical properties, CT-DNA binding and photocatalytic activity. RSC Advances 2020; 10(37):22027-22035.

54. Mali SC, Dhaka A, Githala CK, Trivedi R: Green synthesis of copper nanoparticles using Celastrus paniculatus Willd. leaf extract and their photocatalytic and antifungal properties. Biotechnol rep 2020; 27:e00518.

55. Sreeja C, Philip KA, Shamil K, Asraj O, Sreeja S: Biomediated Green Synthesis of Copper Nanoparticles using Piper nigrum Leaf Extract. J Nanosci Nanotechnol 2020:908-910.

56. Amer M, Awwad A: Green synthesis of copper nanoparticles by Citrus limon fruits extract, characterization and antibacterial activity. 2020.

57. Bawazeer S, Khan I, Rauf A, Aljohani AS, Alhumaydhi FA, Khalil AA, Qureshi MN, Ahmad L, Khan SA: Black pepper (Piper nigrum) fruit-based gold nanoparticles (BP-AuNPs): Synthesis, characterization, biological activities, and catalytic applications–A green approach. Green Process Synth 2022; 11(1):11-28.

58. Nahak G, Sahu R: Phytochemical evaluation and antioxidant activity of Piper cubeba and Piper nigrum. J Applied Pharma Sci 2011; 1(8):153.

59. Alminderej F, Bakari S, Almundarij TI, Snoussi M, Aouadi K, Kadri A: Antimicrobial and wound healing potential of a new chemotype from Piper cubeba L. essential oil and in silico Study on S. aureus tyrosyl-tRNA synthetase protein. Plants 2021; 10(2):205.

60. Shah R, Pathan A, Vaghela H, Ameta SC, Parmar K: Green synthesis and characterization of copper nanoparticles using mixture (Zingiber officinale, Piper nigrum and Piper longum) extract and its antimicrobial activity. Chem Sci Trans 2019; 8(1):63-69

61 Karlsson H, Toprak M, Fadeel B: Handbook on the Toxicology of Metals. In.: Elsevier Amster Netherlands; 2015.

62. Zain NM, Stapley AG, Shama G: Green synthesis of silver and copper nanoparticles using ascorbic acid and chitosan for antimicrobial applications. Carbohydr Polym 2014; 112:195-202.

63. Santo CE, Quaranta D, Grass G: Antimicrobial metallic copper surfaces kill Staphylococcus haemolyticus via membrane damage. Microbiologyopen 2012; 1(1):46-52.

64. Grass G, Rensing C, Solioz M: Metallic copper as an antimicrobial surface. A environ microbiol 2011; 77(5):1541-1547.

65. Macomber L, Imlay JA: The iron-sulfur clusters of dehydratases are primary intracellular targets of copper toxicity. Proc Natl Acad Sci 2009; 106(20):8344-8349.

66. Bona L: Cytotoxic Activity of Piper cubeba: A Review. Int Res J Pharm 2021.

67. Suman T, Rajasree SR, Kanchana A, Elizabeth SB: Biosynthesis, characterization and cytotoxic effect of plant mediated silver nanoparticles using Morinda citrifolia root extract. Colloids Surf B: Biointerfaces 2013; 106:74-78.

68. Jacob SJP, Finub J, Narayanan A: Synthesis of silver nanoparticles using Piper longum leaf extracts and its cytotoxic activity against Hep-2 cell line. Colloids surf B 2012; 91:212-214.

69. Vivek R, Thangam R, Muthuchelian K, Gunasekaran P, Kaveri K, Kannan S: Green biosynthesis of silver nanoparticles from Annona squamosa leaf extract and its in vitro cytotoxic effect on MCF-7 cells. Process Bioche 2012; 47(12):2405-2410.

70. Sankar R, Maheswari R, Karthik S, Shivashangari KS, Ravikumar V: Anticancer activity of Ficus religiosa engineered copper oxide nanoparticles. Mater Sci Eng C 2014; 44:234-239.

71. Greenwell M, Rahman P: Medicinal plants: their use in anticancer treatment. Int J Pharm Sci Res 2015; 6(10):4103.

72. Phaniendra A, Jestadi DB, Periyasamy L: Free radicals: properties, sources, targets, and their implication in various diseases. Indian J Clin Biochem 2015; 30(1):11-26.

73. Hielscher A, Gerecht S: Hypoxia and free radicals: role in tumor progression and the use of engineering-based platforms to address these relationships. Free Radic Biol Med 2015; 79:281-291.

74. Desai AG, Qazi GN, Ganju RK, El-Tamer M, Singh J, Saxena AK, Bedi YS, Taneja SC, Bhat HK: Medicinal plants and cancer chemoprevention. Curr Drug Metab 2008; 9(7):581-591.

75. Gross, C. H., Parsons, J. D., Grossman, T. H., Charifson, P. S., Bellon, S., Jernee, J., … Raybuck, S. A. (2003). Active-site residues of Escherichia coli DNA gyrase required in coupling ATP hydrolysis to DNA supercoiling and amino acid substitutions leading to novobiocin resistance. Antimicrobial Agents and Chemotherapy, 47(3), 1037–1046. https://doi.org/10.1128/AAC.47.3.1037-1046.2003

76. Sharifi-Rad, J., Quispe, C., Durazzo, A., Lucarini, M., Souto, E. B., Santini, A., … Cruz-Martins, N. (2022). Resveratrol' biotechnological applications: Enlightening its antimicrobial and antioxidant properties. Journal of Herbal Medicine, 32. https://doi.org/10.1016/j.hermed.2022.100550

Tables

Tables 1-3 are available in the Supplementary Files section.

Figures

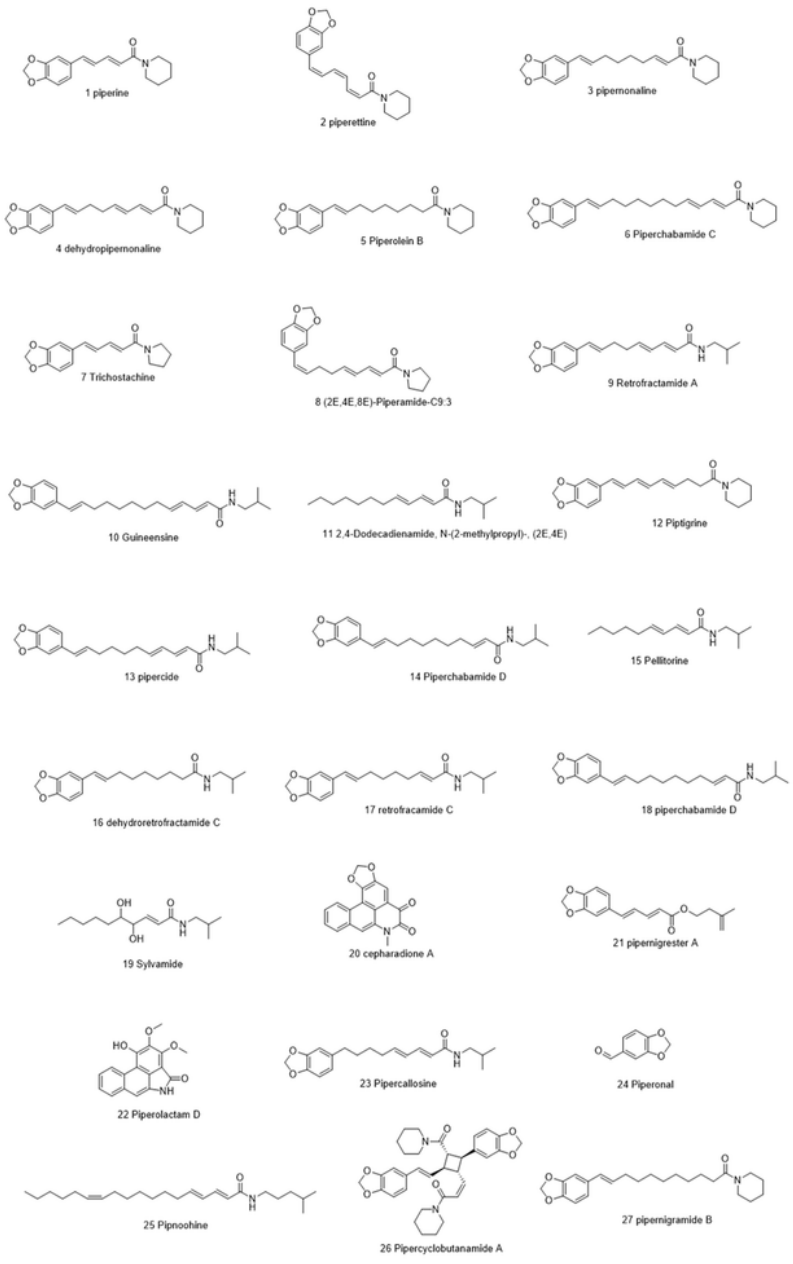

Figure 1

Chemical structures of some selected alkamides in Piper nigrum fruits

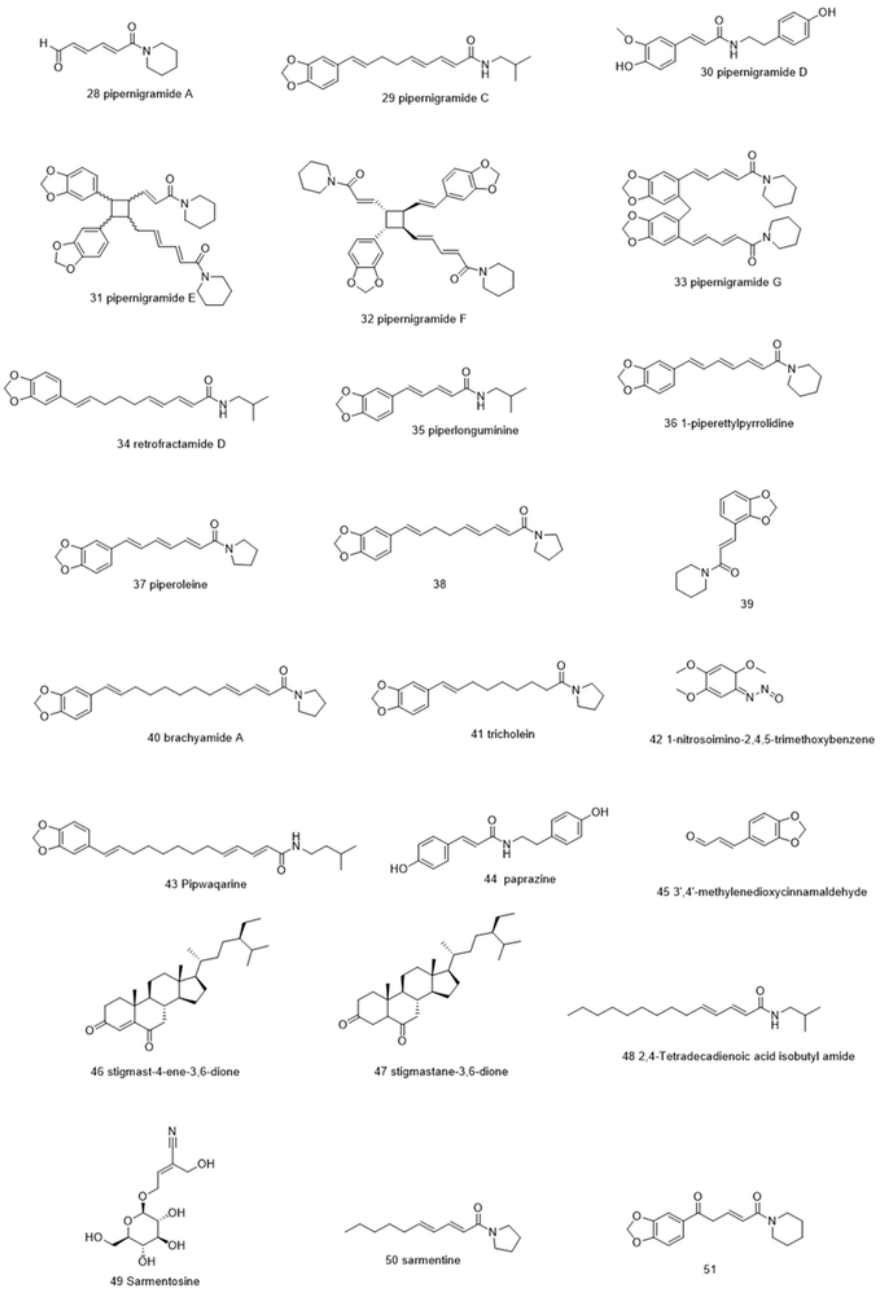

Figure 2

Chemical structures of some selected alkamides in Piper nigrum

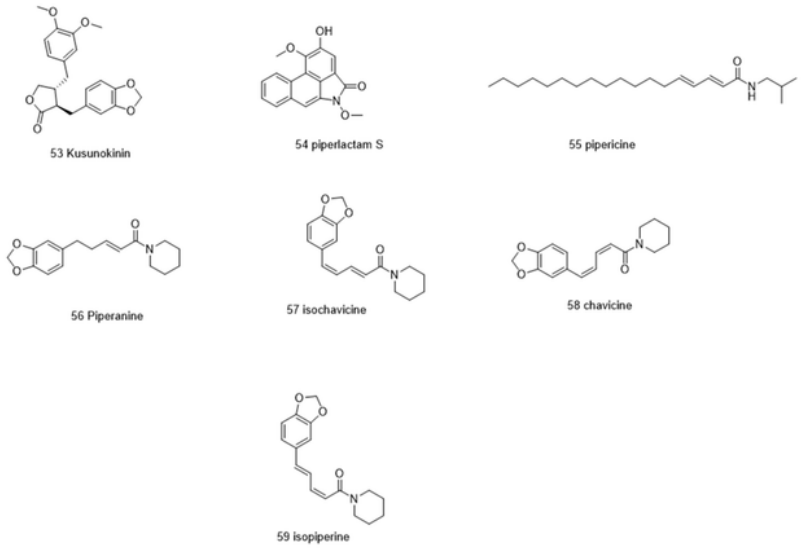

Figure 3

Chemical structures of some selected alkamides in Piper nigrum fruits

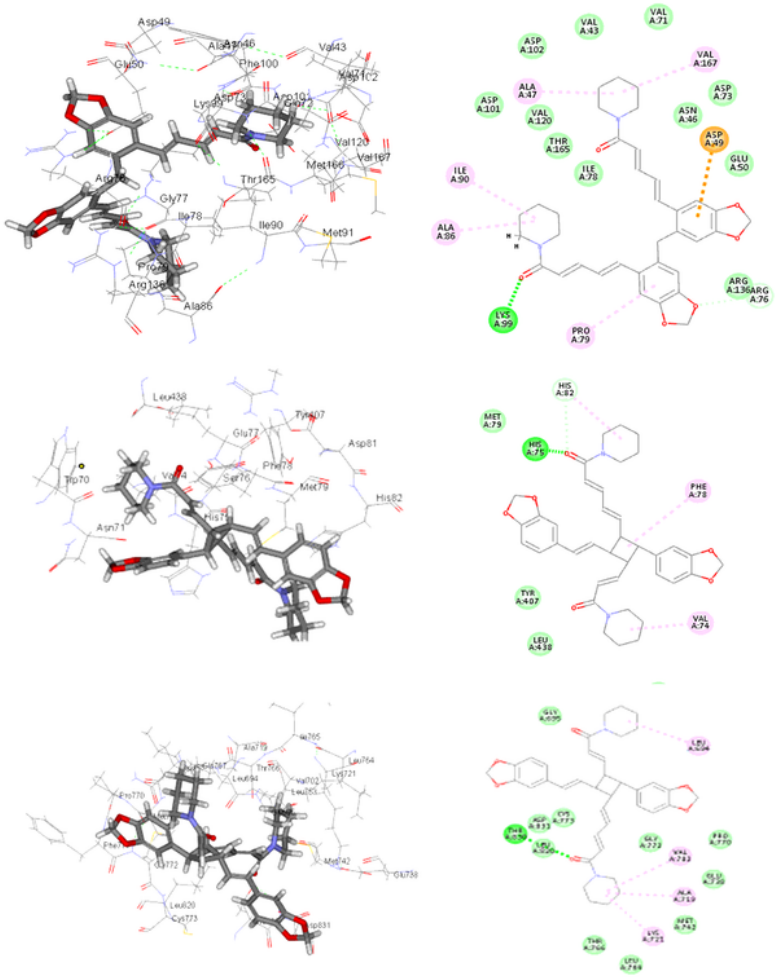

Figure 4

2D and 3D binding of the most potent compound 32 in the binding pockets of A. glutathione reductase B. DNA gyrase topoisomerase II and C. EGFR tyrosine kinase

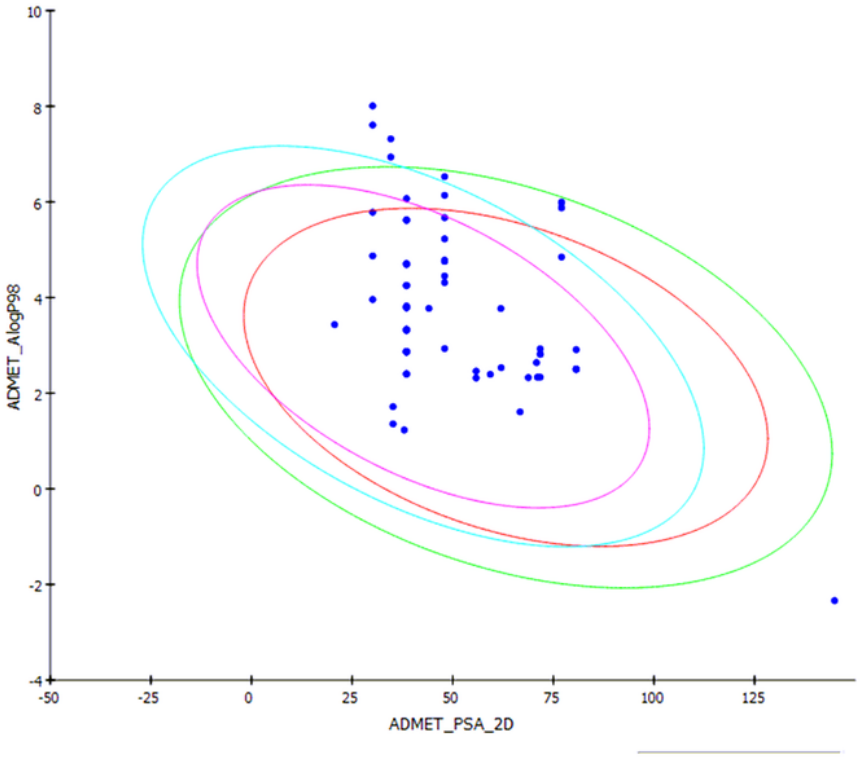

Figure 5

ADMET plot for chosen alkamides from Piper nigrum fruits, showing blood-brain barrier (BBB) 99% and 95% confidence limit ellipses and the human intestinal absorption models in ADMET_AlogP98.

Supplementary Files

This is a list of supplementary files associated with this preprint. Click to download.

- table1.tif
- table2.tif
- table3.tif
- SupplementaryMaterialfinal.docx